

Deep Cuboid Detection: Beyond 2D Bounding Boxes

Debidatta Dwibedi*
 Carnegie Mellon University
 debidatta@cmu.edu

Tomasz Malisiewicz Vijay Badrinarayanan Andrew Rabinovich
 Magic Leap, Inc.
 {tmalisiewicz, vbadrinarayanan, arabinovich}@magic leap.com

Abstract

We present a Deep Cuboid Detector which takes a consumer-quality RGB image of a cluttered scene and localizes all 3D cuboids (box-like objects). Contrary to classical approaches which fit a 3D model from low-level cues like corners, edges, and vanishing points, we propose an end-to-end deep learning system to detect cuboids across many semantic categories (e.g., ovens, shipping boxes, and furniture). We localize cuboids with a 2D bounding box, and simultaneously localize the cuboid’s corners, effectively producing a 3D interpretation of box-like objects. We refine keypoints by pooling convolutional features iteratively, improving the baseline method significantly. Our deep learning cuboid detector is trained in an end-to-end fashion and is suitable for real-time applications in augmented reality (AR) and robotics.

1. Introduction

Building a 3D representation of the world from a single monocular image is an important problem in computer vision. In some applications, we have the advantage of having explicit 3D models and try to localize these objects in the world while estimating their pose. But without such 3D models, we must reason about the world in terms of simple combinations of geometric shapes like cuboids, cylinders, and spheres. Such primitives, referred to as *geons* by Biederman [5], are easy for humans to reason about. Humans can effortlessly make coarse estimates about the pose of these simple geometric primitives and even compare geometric parameters like length, radius or area across disparate instances. While many objects are composed of multiple geometric primitives, a large number of real objects can be well approximated by as little as one primitive.

For example, let us consider a common shape that we see everyday: *the box*. Many everyday objects can geometrically be classified as a box (e.g., shipping boxes, cabinets, washing machines, dice, microwaves, desktop computers).

*Work done as an intern at Magic Leap, Inc. while a student at Carnegie Mellon University

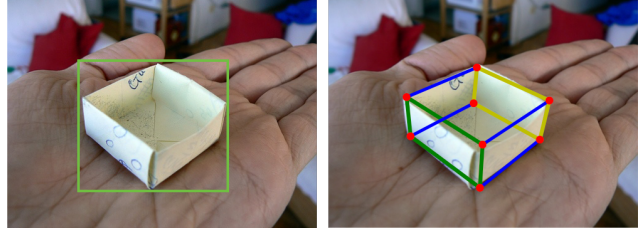


Figure 1. 2D Object detection vs. 3D Cuboid detection. Our task is to find all cuboids inside a monocular image and localize their vertices. Our deep learning system is trained in an end-to-end fashion, runs in real-time, and works on RGB images of cluttered scenes captured using a consumer-grade camera.

Boxes (or cuboids, as we call them in this paper) span a diverse set of everyday object instances, yet it is very easy for humans to fit an imaginary cuboid to these objects and in doing so they localize its vertices and faces. People can also compare the dimensions of different box-like objects even though they are not aware of the exact dimensions or even if the object is not a perfect cuboid. In this work, we specifically deal with the problem of detecting class agnostic geometric entities like cuboids. By class agnostic, we mean that we do not differentiate between a shipping box, a microwave oven, or a cabinet. All of these boxy objects are represented with the same simplified concept called *cuboid* in the rest of the paper.

Detecting boxy objects in images and extracting 3D information like pose helps overall scene understanding. Many high-level semantic problems have been tackled by first detecting boxes in a scene (e.g., extracting the free space in a room by reducing the objects in a scene to boxes [22], estimating the support surfaces in the scene [34, 21] and estimating the scene layout [17]).

A perfect cuboid detector opens up a plethora of possibilities for augmented reality (AR), human-computer interaction (HCI), autonomous vehicles, drones, and robotics in general. The cuboid detector can be used as follows:

- For Augmented Reality, cuboid vertex localization followed by 6-dof pose estimation allows a content cre-

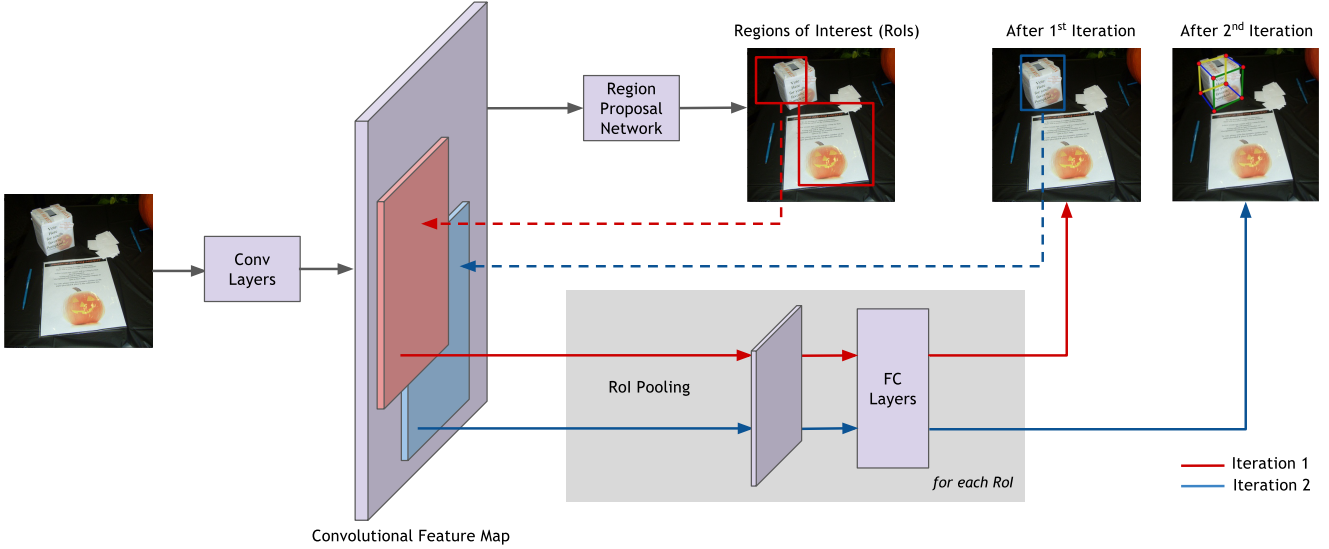


Figure 2. Deep Cuboid Detection Pipeline. The first step is to find Regions of Interest (RoIs) in the image where a cuboid might be present. We train a Region Proposal Network (RPN) to output such regions. Then, features corresponding to each ROI are pooled from a convolutional feature map (*e.g.*, *conv5* in VGG-M). These pooled features are passed through two fully connected layers just like the region-based classification network in Faster R-CNN (see model details in Section 3.1). However, instead of just producing a 2D bounding box, we also output the normalized offsets of the vertices from the center of the region. Finally, we refine our predictions by performing iterative feature pooling (see Section 5.2). The dashed lines show the regions from which features will be pooled.

ator to use the cuboid-centric coordinate system defined by a stationary box to drive character animation. Because we also know the volume of space occupied by the stationary cuboid, animated characters can jump on the box, hide behind it, and even start drawing on one of the box’s faces.

- For Human-Computer Interaction, a hand-held cuboid can be used as a lightweight game controller. A stationary camera observing the hand-held cube is able to estimate the cube’s pose, effectively tracking the cube in 3D space. In essence, the cuboid can serve as a means to improve interaction in AR systems(*e.g.*, the tabletop AR demo using cuboids [57]).
- For autonomous vehicles, 3D cuboid detection allows the vehicle to reason about the spatial extent of rare objects that might be missing in supervised training set. By reasoning about the pose of objects in a class-agnostic manner, autonomous vehicles can be safer drivers.
- For drones, man-made structures such as buildings and houses can be well-approximated with cuboids, assisting navigation during unmanned flights.
- For robotics in general, detecting boxy objects in images and extracting their 3D information like pose helps overall scene understanding. Placing a handful

of cuboids in a scene (instead of Aruco markers) can make pose tracking more robust for SLAM applications.

In general, one can formulate the 3D object detection problem as follows: fit a 3D bounding box to objects in an RGB-D image [48, 49, 34, 46], detect 3D keypoints in an RGB image [51, 53], or perform 3D model to 2D image alignment [50, 24, 2]. In this paper, we follow the keypoint-based formulation. Because an image might contain multiple cuboids as well as lots of clutter, we must first procure a shortlist of regions of interest that correspond to cuboids. In addition to the 2D bounding box enclosing the cuboid, we estimate the location of all 8 vertices.

1.1. From Object Detection to Cuboid Detection

Deep learning [37] has revolutionized image recognition in the past few years. Many state-of-the-art methods in object detection today are built on top of deep networks that were trained for the task of image classification. Not only has the accuracy of object detection increased, there are many approaches that also run in real-time [20, 43, 40]. We take advantage of these advances to detect boxy objects in a scene. Unlike the usual task of object detection, we want more than the bounding box of the object. Instead, we want to localize the vertices of the cuboids (see Figure 1). Another aspect where we differ from the object detection task is that we do not care about the class of the cuboids that

we are detecting. For our purpose, we deal with only two classes: cuboid and not-a-cuboid.

Even if a cuboid is a geometric object that can be easily parameterized, we advocate the use of deep learning to detect them in scenes. Classically, one approach to detect cuboids is to detect the edges and try to fit the model of a cuboid to these edges. Hence, robust edge selection is an important step. However, this becomes difficult when there are misleading textures on cuboidal surfaces, if edges and corners are occluded or the scene contains considerable background clutter. It is a difficult task to classify whether a given line belongs to a given cuboid with purely local features. Hence, we propose to detect cuboids the same way we detect classes like cars and aeroplanes in images, using a data-driven approach. However, the task of fitting a single label 'cuboid' to boxy objects in the scene is not trivial as the label is spread over many categories like houses, washing machines, ballot boxes, etc. In our experiments, we show how a CNN is successful to learn features that help us identify cuboids in different scenes.

1.2. Our Contributions

Our main contribution is a deep learning model that jointly performs cuboid detection and vertex localization. We explore various ways to improve the detection and localization accuracy produced by a baseline CNN. The key idea is to first detect the object of interest and then make coarse predictions regarding the location of its vertices. The next stage acts as an attention mechanism, performing refinement of vertices by only looking at regions with high probability of being a cuboid. We improve localization accuracy with an iterative feature pooling mechanism (see Section 5.2), study the effect of combining cuboid-related losses(see Section 5.1), experiment with alternate parametrizations (see Section 6), and study the effect of different size base networks (see Section 5.4).

2. Related Work

Classical ideas on 3D scene and object recognition originate in Robert's Blocks-World [44] and Biederman's Recognition-by-Components [5]. These early works were overly reliant on bottom-up image processing, thus never worked satisfactorily on real images. Many modern approaches utilize a large training database of 3D models and some kind of learning for 2d-to-3d alignment [1, 2, 53, 9].

Cuboid detection has also been approached with geometry-based methods [52, 28, 38, 22]. Shortly after the success of Deformable Parts Model, researchers extended HOG-based models to cuboids [55, 15]. RGB-D based approaches to cuboid detection are also common [35].

Our work revisits the problem of cuboid detection that Xiao *et al.* introduced in [55]. They use a Deformable Parts-based Model that uses HOG classifiers to detect cuboid

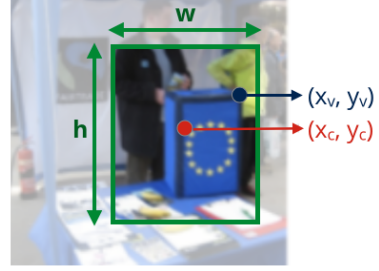


Figure 3. **RoI-Normalized Coordinates** Vertices are represented as offsets from the center of the RoI and normalized by the region's width/height. (x_v, y_v) is a vertex and (x_c, y_c) is the center.

vertices in different views. Their model has four components for scoring a final cuboid configuration: score from the HOG classifier, 2D vertex displacement, edge alignment score and a 3D shape score that takes into account how close the predicted vertices are to a cuboid in 3D. Their approach jointly optimizes over visual evidence (corners and edges) found in the image while penalizing the predictions that stray too far from an actual 3D cuboid. A major limitation of their approach is the computationally expensive test-time iterative optimization step. Not only is their HOG-based model inferior to its modern CNN-based counterpart (as we demonstrate in our experiments), their approach takes more than a minute to process a single image.

Today the best methods in object detection owe their performance to convolutional neural networks. Krizhevsky *et al.* [37] showed that CNNs were superior to existing methods for the task of image classification. To localize an object in an image, the image is broken down into regions and these regions are classified instead. This approach was first shown to work in [20]. This was followed by attempts to make object detection work almost real-time [19, 43]. More recently, researchers have been able to make object detection faster by performing detection in a single step [40, 42]. These approaches run at about 50-60 frames per second which opens up the possibility for adapting such network architectures to real-time cuboid localization.

3D object localization using keypoints is commonly studied [45, 30, 31, 10, 39, 11]. 3D keypoint detection using deep networks is also gaining popularity [53, 51]. There has been a resurgence in work that aims to align 3D models of objects in single view images [23, 36, 54].

The iterative vertex refinement component of our approach is similar to the iterative error feedback approach of [7], the network cascades in [12], the iterative bounding box regression of Multi-region CNN [18] and Inside-Outside Networks [4]. Such iterative models have been reinterpreted as Recurrent Neural Networks in [3, 6], and while most applications focus on human pose estimation, the ideas can easily be extended to cuboid detection.



Figure 4. **Deep Cuboid Detections using VGG16 + Iterative.** Our system is able to localize the vertices of cuboids in consumer-grade RGB images. We can handle both objects like boxes (that are perfectly modeled by a cuboid) as well as objects like sinks (that are only approximate cuboids). Last row: failures of our system (see 6 for more details).

3. Deep Cuboid Detection

We define any geometric shape as a tuple of N parameters. These parameters might be geometric in nature like the radius of a sphere or the length, width and height of a cuboid. However, a more general way to parameterize any geometric primitive is to represent it as a collection of points on the surface of the primitive. If we choose a random point on the surface of the primitive, it might not necessarily be localizable from a computer-vision point of view. Ideally, we want the set of parametrization points to be *geometrically informative* and *visually discriminative* [16]. Specifically, in the case of cuboids, these special keypoints are the same as the cuboid’s corners.¹

We define a cuboid as a tuple of 8 vertices where each point is denoted by its coordinates (x, y) in the image. In our default parametrization, we use the 16 coordinate parameters to represent a cuboid in an image. This, however, is an overparameterization as 16 parameters are not required to represent a cuboid (see Section 6 for a discussion on al-

¹When discussing cuboids, we use the terms vertex, corner, and keypoint, interchangeably.

ternate cuboid parametrizations).

3.1. Network Architecture and Loss Functions

Our network is made up of several key components: the CNN Tower, the Region Proposal Network (RPN), R-CNN classifier and regressor, and a novel iterative feature pooling procedure which refines cuboid vertex estimates. Our architecture is visually depicted in Figure 2.

1. The CNN Tower is the pre-trained fully convolutional part of popular ConvNets like VGG and ResNets. We refer to the last layer of the tower as the convolutional feature map (e.g., conv5 in VGG16 is of size $M \times N \times 512$).
2. The RPN is a fully convolutional network that maps every cell in the feature map to a distribution over K multi-scale anchor-boxes, bounding box offsets, and objectness scores. The RPN has two associated losses: log loss for objectness and smooth L1 for bounding box regression. Our RPN uses 512 3×3 filters, then 18 1×1 filters for objectness and 36 1×1 filters for bounding box offsets. (See Faster R-CNN [43] for more details.)
3. The ROI pooling layer uses max pooling to convert the features inside any valid region of interest into a small fixed-size feature map. E.g., for conv5 of size $M \times N \times 512$, the pooling layer produces an output of size $7 \times 7 \times 512$, independent of the input regions aspect ratio and scale. ROI pooling is the non-hierarchical version of SPPNet [27].
4. The RCNN regressor is then applied to each fixed-size feature vector, outputting a cuboidness score, bounding box offsets (4 numbers), and 8 cuboid vertex locations (16 numbers). The bounding box regression values ($\Delta x, \Delta y, \Delta w, \Delta h$) [19] are used to fit the initial object proposal tightly around the object. The vertex locations are encoded as offsets from the center of the ROI and are normalized by the proposal width/height as shown in Figure 3. The ground truth targets for each vertex are:

$$t_x = \frac{x_v - x_c}{w}, t_y = \frac{y_v - y_c}{h}$$

The RCNN uses two fully connected layers (4096 neurons each), and has three associated losses: log loss for cuboidness and smooth L_1 for both bounding box and vertex regression.

5. When viewed in unison, the ROI pooling and RCNN layers act as a refinement mechanism, mapping an input box to an improved one, given the feature map.

This allows us to apply the last part of our network multiple times — a step we call iterative feature pooling (See section 5.2).

The loss function used in the RPN consists of $L_{anchor-cls}$, the log loss over two classes (cuboid vs. not cuboid) and $L_{anchor-reg}$, the Smooth L_1 loss [19] of the bounding box regression values for each anchor box. The loss function for the R-CNN is made up of $L_{ROI-cls}$, the log loss over two classes (cuboid vs. not cuboid), $L_{ROI-reg}$, the Smooth L_1 loss of the bounding box regression values for the ROI and $L_{ROI-corner}$, the Smooth L_1 loss over the ROI’s predicted vertex locations. We also refer to the last term as the corner regression loss. In the experiments section, we report how adding these additional tasks affects the detector performance (see Table 1).

The complete loss function is a weighted sum of the above mentioned losses and can be written as follows:

$$L = \lambda_1 L_{anchor-cls} + \lambda_2 L_{anchor-reg} + \\ \lambda_3 L_{ROI-cls} + \lambda_4 L_{ROI-reg} + \lambda_5 L_{ROI-corner}$$

We use Caffe [33] for our experiments and build on top of the implementation of Faster R-CNN by Girshick *et al.* [19]. For all experiments we start with either the VGG-M [8] or VGG16 [47] networks that have been pre-trained for the task of image classification on ImageNet. VGG-M is a smaller model with 7 layers while VGG16 contains 16 layers. We fine-tune all models for 50K iterations using SGD with a learning rate of 0.001 and reduce the learning rate by a factor of 10 after 30K iterations. We also use a momentum of 0.9, weight decay of 0.0005 and dropout of 0.5. We do not perform any stage-wise training. Instead, we jointly optimize over all tasks and have kept the value of all the loss weights as one in our experiments (*i.e.*, $\lambda_i = 1$).

4. Data

We use the SUN Primitive dataset [55] to train our deep cuboid detector. This is the largest publicly available cuboid dataset — it consists of 3516 images and is a mix of indoor scenes with lots of clutter, internet images containing only a single cuboid and outdoor images of buildings that also look like cuboids. Both cuboid bounding boxes and cuboid vertices have ground-truth annotations. In this dataset, we have 785 images with 1269 annotated cuboids. The rest of the images are negatives — they do not contain any cuboids. We make a split to create a training set of 3000 images and 516 test images. We augment the 3000 images with their horizontally flipped versions while training, but cuboid-specific data augmentation [29] strategies are likely to further improve performance.

Additional loss function	AP	APK	PCK
Bounding Box Loss	66.33	-	-
Corner Loss	58.39	28.68	27.64
Bounding Box + Corner Loss	67.11	34.62	29.38

Table 1. **Multi-task learning Results** We first train a network using only the bounding box loss, then use the cuboid corner loss.

5. Experiments

We evaluate the system on two tasks: cuboid bounding box detection and cuboid keypoint localization. For detection, a bounding box is correct if the Intersection over Union (IoU) overlap is greater than 0.5.². Detections are sorted by confidence (the network’s classifier softmax output) and we report the mean Average Precision (AP) as well as the entire Precision-Recall curve. For keypoint localization we use the Probability of Correct Keypoint (PCK) and Average Precision of Keypoint (APK) metrics [56]. PCK and APK are commonly used in the human pose estimation literature to measure the performance of systems predicting the location of human body parts like head, wrist, etc. PCK measures the fraction of annotated instances that are correct when all the ground truth boxes are given as input to the system. A predicted keypoint is correct if its normalized distance from the annotation is less than a threshold (α). APK, on the other hand, takes both detection confidence and keypoint localization into consideration. We use a normalized distance, α , of 0.1 which means that a predicted keypoint is considered to be correct if it lies within $0.1 \times \max(\text{height}, \text{width})$ pixels of the ground truth annotation of the keypoint. See Figure 7 to see these metrics reported on the SUN Primitive test set and samples of cuboid detections in Figure 4.

For bounding box detection, our best network architecture achieves a mAP of 75.47, which is significantly better than the HOG-based system of Xiao *et al.* [55] which reports a mAP of 24.0.

5.1. Multi-task learning

We train multiple networks each of which performs different multiple tasks. We start off with a base network that just outputs bounding boxes around cuboids — that is we train a network to perform general object detection using just the rectangle enclosing the cuboids. The above network outputs the class of the box and the bounding box regression values. Next, we train a different model with additional supervision about the location of the corners but this model does not output bounding box regression coordinates. Finally, we train a network that outputs both the bounding box regression values and the coordinates of the vertex. A cor-

²This is the standard way to evaluate a 2D object detector as was popularized by the PASCAL VOC object detection challenge [14]

Method	AP	APK	PCK
Corner Loss	58.39	28.68	27.64
Corner Loss + Iterative	62.89	33.98	35.56
BB+Corner Losses	67.11	34.62	29.38
BB+Corner Loss + Iterative	71.72	37.61	36.53

Table 2. **Results for Iterative Feature Pooling.** Our iterative algorithm improves the box detection AP by over 4% and PCK over 7%.

responding term is added to the loss function for each additional task. From our experiments, we can see how adding more tasks affects the performance of the cuboid detector (see Table 1).

5.2. Iterative Feature Pooling

In R-CNN, the final output is a classification score and the bounding box regression values for every region proposal. The bounding box regression allows us to move the region proposal around and scale it such that the final bounding box localizes just the object. This implies that our initial region from which we pooled features to make this prediction was not entirely correct. Hence, it makes sense to go back and pool features from the correct bounding box. We implement this in the network itself which means that we perform iterative bounding box regression while training and testing in exactly the same way. The input to the fully-connected layers is a fixed-size feature map that consists of the pooled features from different region proposals from *conv5* layer. The R-CNN outputs are used for bounding box regression on the input object proposals to produce new proposals. Then features are pooled from these new proposals and passed through the fully-connected layers again. This model is now an “any-time prediction system” where for applications which are not bound by latency, bounding box regression can be performed more than once. Our results (see Table 2) show that iterative feature pooling can greatly improve both bounding box detection and vertex localization (see Figure 5). There isn’t a significant change in performance when we iteratively pool features more than twice.

5.3. Depth of Network

We experiment with two base models: VGG16 and VGG-M. While VGG16 has a very deep architecture with 16 layers, VGG-M is a smaller model with 7 layers. We report results of these experiments in Table 3. Interestingly, for this dataset and task, two iterations through the shallower network outperforms one iteration through the deeper network. Coupled with the fact the shallower network with iteration runs twice as fast, it can be a good choice for deployment.

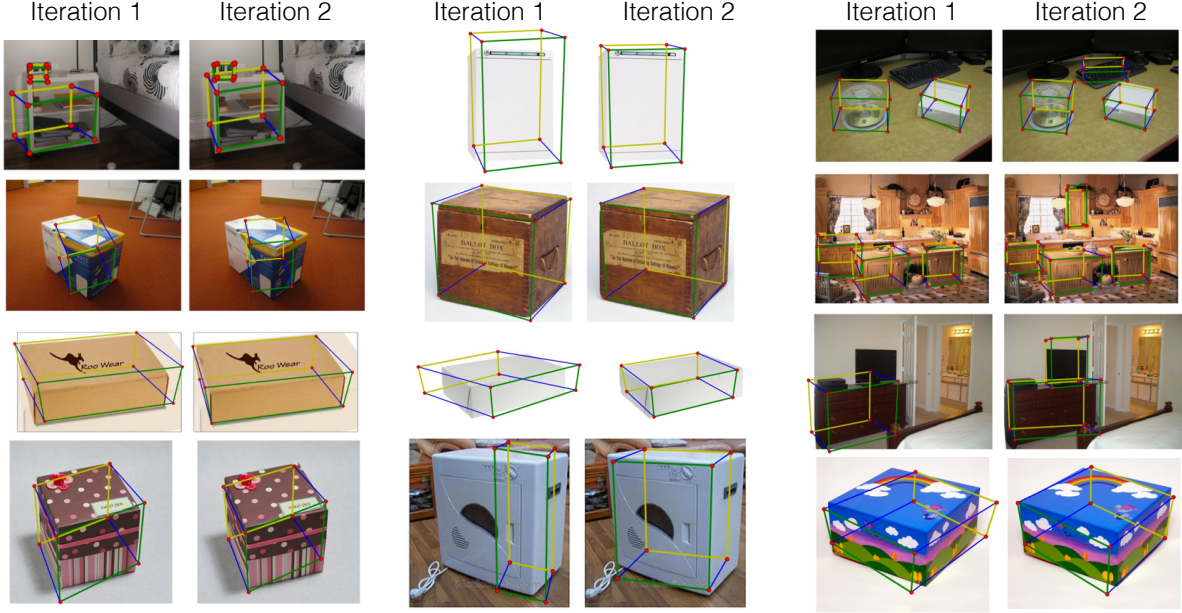


Figure 5. **Vertex Refinement via Iterative Feature Pooling.** We refine cuboid detection regions by re-pooling features from *conv5* using the predicted bounding boxes (see Section 5.2).

Method	AP	APK	PCK	Size	Speed
VGG-M	67.11	34.62	29.38	334MB	14fps
VGG-M + I	71.72	37.61	36.53	334MB	10fps
VGG16	70.50	33.65	35.83	522MB	5fps
VGG16 + I	75.47	41.21	38.27	522MB	4fps

Table 3. **VGG-M (7 layer) vs. VGG16 (16 layer) base network.** I implies iterative feature pooling was performed. The deeper cuboid detector outperforms the shallower one.

Number of Images	AP	APK	PCK
1000	40.47	20.83	26.60
2000	52.17	27.51	29.31
3000	71.72	37.61	36.53

Table 4. **Performance vs. number of training images.** Deep cuboid detection benefits from more training images.

5.4. Effect of Training Set Size

We wanted to measure the impact of increasing the size of training data. We create three datasets of varying sizes: 1K, 2K and 3K images and train a common network (VGG-M + Iterative). Our results (see Table 4) show significantly improved performance when using larger training set sizes.

5.5. Memory and Runtime Complexity

Our cuboid detector is able to run at interactive rates on a Titan Z GPU while the HOG-based approach of Xiao *et*

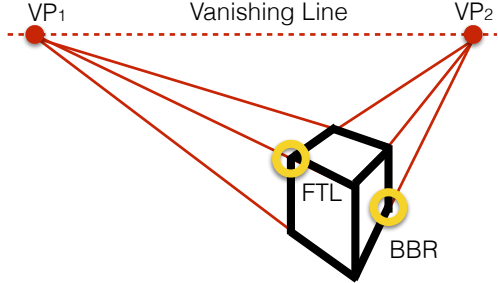
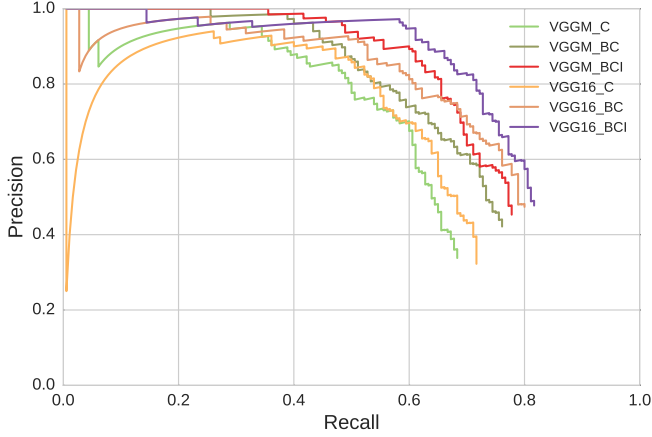


Figure 6. **Cuboid Vanishing Points.** Vanishing points produced by extrapolating the edges of a cube can be used to reduce the number of parameters. We can drop the Front-Top-Left (FTL) and Back-Bottom-Right (BBR) vertices from our parametrization, and infer them using estimated VPs.

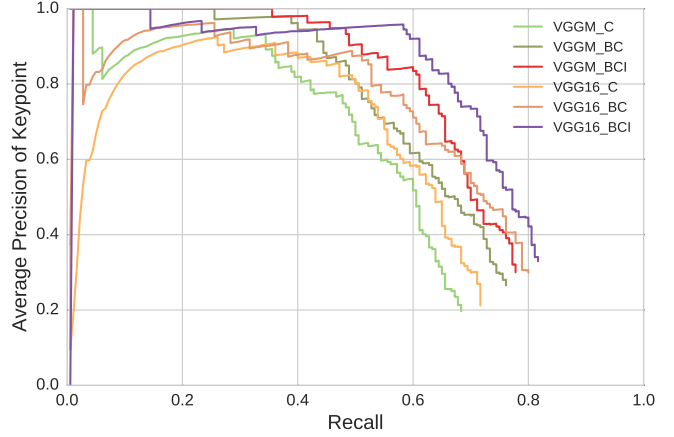
al. [55] takes minutes to process a single image. The real-time nature of the system is due to the fact that our implementation is based on top of Faster R-CNN. We anticipate that progress in object detection like SSD [40] can be leveraged to have a cuboid detector that is even faster. We also report the model size in MB (see Table 3). Further optimization can be done to reduce the size of the model such that it fits on mobile devices [41, 32, 25].

6. Discussion

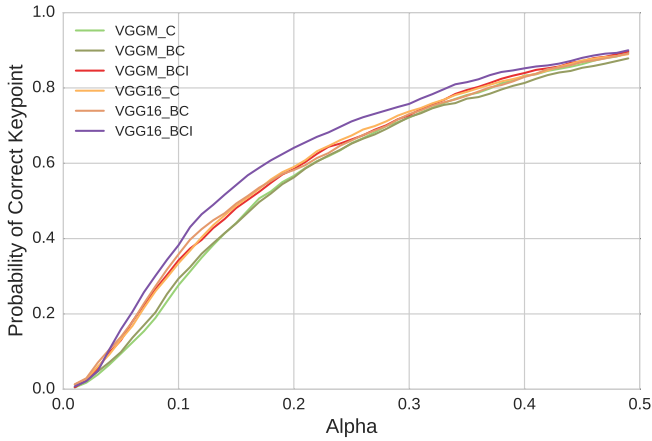
So far, all of our networks output the cuboid’s 8 vertices directly. However, a closer look at typical failures sug-



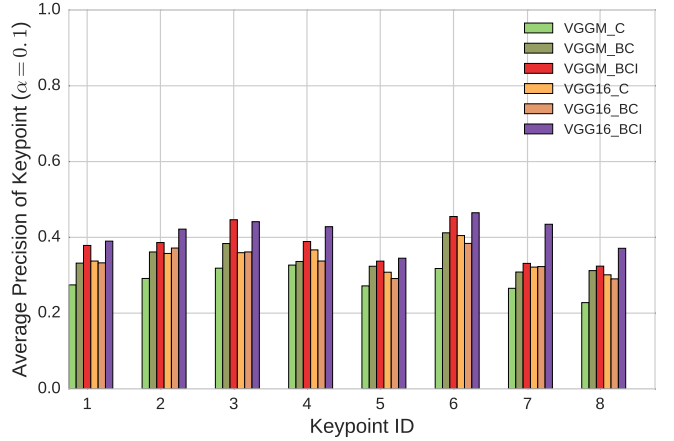
(a) Precision-Recall Curve



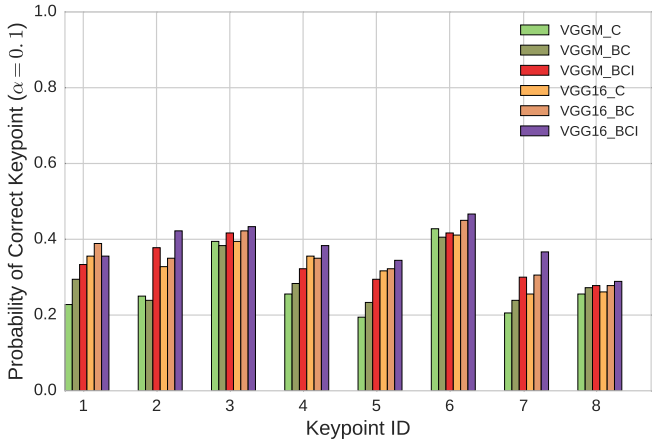
(b) APK vs. Recall



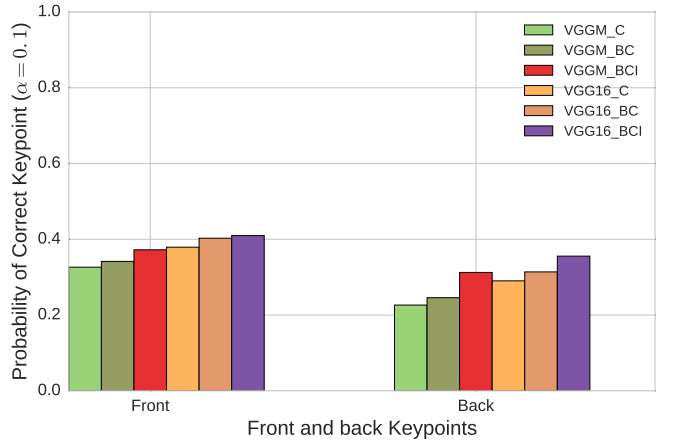
(c) PCK vs. α



(d) Keypoint-wise APK



(e) Keypoint-wise PCK



(f) Face-wise PCK

Figure 7. Deep Cuboid Detector Evaluation Metrics. APK: Average Precision of Keypoint, PCK: Probability of Correct Keypoint, α : Normalized distance from GT corners, Order of keypoints: front-top-left, back-top-left, front-bottom-left, front-top-right, back-bottom-left, front-bottom-right, back-top-right, back-bottom-right. B = Bounding box loss, C = Corner loss, I = Iterative.

Method	AP	APK	PCK	PCK of BBR Corner	PCK of FTL Corner	PCK of Remaining Corners
6 corners	65.26	29.64	27.36	24.44	21.11	28.89
8 corners	67.11	34.62	29.38	27.22	29.44	29.73

Table 5. **8 corner vs. 6 corner parameterization** The 8 corner parameterization uses all of the cuboid’s corners, whereas in the 6 corner version, the BBR and FTL corners are dropped (see Figure 6) and inferred from the vanishing points. This shows how the network is able to do geometric reasoning and the over-parameterization adds robustness to the system (see Section 6). **BBR:** Back-Bottom-Right and **FTL:** Front-Top-Left

gests that our parametrization might be to blame. Certain viewpoints have an inherent ambiguity (e.g., which face of the Rubiks cube in Figure 4 should be labelled the front?). Since our detector has trouble dealing with such configurations, in this section we explore and discuss alternate cuboid parametrizations. If we consider the world origin to coincide with camera center coordinates, the minimal parameterization of the cuboid can be done with 12 numbers:

- (X, Y, Z) - Centre of cuboid in 3D
- (L, W, H) - Dimensions of the cuboid
- (θ, ψ, ϕ) - 3 angles of rotation of the cuboid
- (f, c_x, c_y) - Intrinsic camera parameters

For modern cameras, we can assume there is no skew in the camera and equal focal lengths. The over-parameterization we have in our network (as we predict 16 numbers) allows the network to produce outputs that do not represent cuboids. We experimented with several different re-parameterizations of a cuboid in an attempt to better utilize the geometric constraints. In general, our observation is that the network is able to learn features for tasks that have more visual evidence in the image and predict parameters which can be scaled properly for stable optimization. When dealing with 3D geometry and deep learning, proper parametrization is important. Even image-to-image transformations like homographies benefit from re-parametrization (e.g., the 4-point parametrization [13]).

6-corner parametrization: We explore an alternate parameterization in which we predict only 6 coordinates and infer the locations of the remaining two coordinates using the fact that there are parallel edges in cuboids. The edges that are parallel in 3D meet at the vanishing point in the image. There are two pairs of parallel lines on the top and bottom face of the cuboid. These lines should meet at the same vanishing point [26] as shown in Figure 6. Using this fact, we can infer the position of the remaining two points. This allows us to parameterize our output in 12 numbers.

We carry out an experiment to be able to compare the 8 corner parameterization with the 6 corner parameterization. To do so, we decide to not use the ground truth data for two vertices while training. We leave one vertex each from the back and front faces (those whose detection rates

(PCK) were the worst). We train a network to predict the location of the remaining 6 corners. We infer the location of the two dropped vertices using these 6 corners. We do so by first finding out the vanishing points corresponding to the 6 points we predicted. This reparameterization, however, leads to a reduction in performance (see Table 5). This degradation is due to the fact that we discard any visual evidence corresponding to the two inferred corners present in the image. Also, any error in prediction of one vertex due to occlusion or any other reason is directly propagated to the inferred corners. However, left to the CNN it learns multiple models to detect a cuboid. The network is free to use all visual evidence to localize the corners of the cuboid. It is interesting to note that a CNN is capable of doing pure geometric reasoning because in many cases the corner on the back does not have visual evidence in the image due to self-occlusion.

Vanishing point parametrization: Another re-parameterization³ uses locations of the two vanishing points and the slopes of six lines which will form the edges of the cuboid (see Figure 6). Note that these vanishing points correspond to a particular cuboid and might be different from the vanishing point of the entire image. The intersection points of these 6 lines would give us the vertices of the cuboid. However, the network fails to learn the location of the vanishing points as many a time they lie outside the region of interest and have little or confounding visual evidence in the region of interest or the entire image itself. It also becomes difficult to normalize the targets to predict the vanishing points directly. The slopes of the 6 lines can vary between $-\infty$ to $+\infty$. Instead of predicting the slope directly, we tried to regress to value of $\sin(\tan^{-1}(\theta))$. We found it difficult to train the network with this parameterization but there might exist a set of hyperparameters (loss weights, learning rates, solver, etc) for which we can train the above mentioned network.

7. Conclusion

In this paper we have presented an end-to-end deep learning system capable of detecting cuboids and localizing their vertices in RGB images of cluttered scenes. By casting

³The standard parameterization involves predicting the 8 vertices (16 parameters) of the cuboid directly.

the problem in a modern end-to-end deep learning framework, there is no need to design custom low-level detectors for line segments, vanishing points, junctions, etc. With Augmented Reality and Robotics applications in mind, we hope that the design and architecture of our system will inspire researchers to improve upon our results. Future work will focus on: training from much larger datasets and synthetic data, network optimization, and various regularization techniques to improve generalization.

References

- [1] M. Aubry, D. Maturana, A. A. Efros, B. C. Russell, and J. Sivic. Seeing 3d chairs: exemplar part-based 2d-3d alignment using a large dataset of cad models. In *Proceedings of the IEEE Conference on Computer Vision and Pattern Recognition*, pages 3762–3769, 2014. [3](#)
- [2] A. Bansal, B. Russell, and A. Gupta. Marr revisited: 2d-3d alignment via surface normal prediction. In *CVPR*, 2016. [2](#), [3](#)
- [3] V. Belagiannis and A. Zisserman. Recurrent human pose estimation. *arXiv preprint arXiv:1605.02914*, 2016. [3](#)
- [4] S. Bell, C. L. Zitnick, K. Bala, and R. Girshick. Inside-outside net: Detecting objects in context with skip pooling and recurrent neural networks. In *CVPR*, 2016. [3](#)
- [5] I. Biederman. Recognition-by-components: a theory of human image understanding. *Psychological review*, 94(2):115, 1987. [1](#), [3](#)
- [6] A. Bulat and G. Tzimiropoulos. Human pose estimation via convolutional part heatmap regression. In *ECCV*, pages 717–732. Springer, 2016. [3](#)
- [7] J. Carreira, P. Agrawal, K. Fragkiadaki, and J. Malik. Human pose estimation with iterative error feedback. In *CVPR*, 2016. [3](#)
- [8] K. Chatfield, K. Simonyan, A. Vedaldi, and A. Zisserman. Return of the devil in the details: Delving deep into convolutional nets. *arXiv preprint arXiv:1405.3531*, 2014. [5](#)
- [9] C. B. Choy, D. Xu, J. Gwak, K. Chen, and S. Savarese. 3d-r2n2: A unified approach for single and multi-view 3d object reconstruction. In *ECCV*, 2016. [3](#)
- [10] A. Collet, M. Martinez, and S. S. Srinivasa. The moped framework: Object recognition and pose estimation for manipulation. *The International Journal of Robotics Research*, 30(10):1284–1306, 2011. [3](#)
- [11] A. Crivellaro, M. Rad, Y. Verdie, K. Moo Yi, P. Fua, and V. Lepetit. A novel representation of parts for accurate 3d object detection and tracking in monocular images. In *Proceedings of the IEEE International Conference on Computer Vision*, pages 4391–4399, 2015. [3](#)
- [12] J. Dai, K. He, and J. Sun. Instance-aware semantic segmentation via multi-task network cascades. In *CVPR*, 2016. [3](#)
- [13] D. DeTone, T. Malisiewicz, and A. Rabinovich. Deep image homography estimation. *arXiv preprint arXiv:1606.03798*, 2016. [9](#)
- [14] M. Everingham, L. Van Gool, C. K. Williams, J. Winn, and A. Zisserman. The pascal visual object classes (voc) challenge. *International journal of computer vision*, 88(2):303–338, 2010. [6](#)
- [15] S. Fidler, S. Dickinson, and R. Urtasun. 3d object detection and viewpoint estimation with a deformable 3d cuboid model. In *Advances in neural information processing systems*, pages 611–619, 2012. [3](#)
- [16] D. F. Fouhey, A. Gupta, and M. Hebert. Data-driven 3d primitives for single image understanding. In *Proceedings of the IEEE International Conference on Computer Vision*, pages 3392–3399, 2013. [4](#)
- [17] A. Geiger, C. Wojek, and R. Urtasun. Joint 3d estimation of objects and scene layout. In *Advances in Neural Information Processing Systems*, pages 1467–1475, 2011. [1](#)
- [18] S. Gidaris and N. Komodakis. Object detection via a multi-region and semantic segmentation-aware cnn model. In *Proceedings of the IEEE International Conference on Computer Vision*, pages 1134–1142, 2015. [3](#)
- [19] R. Girshick. Fast r-cnn. In *ICCV*, pages 1440–1448, 2015. [3](#), [5](#)
- [20] R. Girshick, J. Donahue, T. Darrell, and J. Malik. Rich feature hierarchies for accurate object detection and semantic segmentation. In *Proceedings of the IEEE conference on computer vision and pattern recognition*, pages 580–587, 2014. [2](#), [3](#)
- [21] A. Gupta, A. A. Efros, and M. Hebert. Blocks world revisited: Image understanding using qualitative geometry and mechanics. In *European Conference on Computer Vision*, pages 482–496. Springer, 2010. [1](#)
- [22] A. Gupta, S. Satkin, A. A. Efros, and M. Hebert. From 3d scene geometry to human workspace. In *Computer Vision and Pattern Recognition (CVPR), 2011 IEEE Conference on*, pages 1961–1968. IEEE, 2011. [1](#), [3](#)
- [23] S. Gupta, P. Arbeláez, R. Girshick, and J. Malik. Aligning 3d models to rgb-d images of cluttered scenes. In *Proceedings of the IEEE Conference on Computer Vision and Pattern Recognition*, pages 4731–4740, 2015. [3](#)
- [24] S. Gupta, P. Arbeláez, R. Girshick, and J. Malik. Inferring 3d object pose in rgb-d images. *arXiv preprint arXiv:1502.04652*, 2015. [2](#)
- [25] S. Han, H. Mao, and W. J. Dally. Deep compression: Compressing deep neural network with pruning, trained quantization and huffman coding. In *ICLR*, 2016. [7](#)
- [26] R. Hartley and A. Zisserman. *Multiple view geometry in computer vision*. Cambridge university press, 2003. [9](#)
- [27] K. He, X. Zhang, S. Ren, and J. Sun. Spatial pyramid pooling in deep convolutional networks for visual recognition. In *European Conference on Computer Vision*, pages 346–361. Springer, 2014. [5](#)
- [28] V. Hedau, D. Hoiem, and D. Forsyth. Recovering free space of indoor scenes from a single image. In *Computer Vision and Pattern Recognition (CVPR), 2012 IEEE Conference on*, pages 2807–2814. IEEE, 2012. [3](#)
- [29] M. Hejrati and D. Ramanan. Categorizing cubes: Revisiting pose normalization. In *2016 IEEE Winter Conference on Applications of Computer Vision (WACV)*, pages 1–9. IEEE, 2016. [5](#)
- [30] D. Hoiem and S. Savarese. Representations and techniques for 3d object recognition and scene interpretation. *Synthesis Lectures on Artificial Intelligence and Machine Learning*, 5(5):1–169, 2011. [6](#)

- [31] E. Hsiao, A. Collet, and M. Hebert. Making specific features less discriminative to improve point-based 3d object recognition. 3
- [32] F. N. Iandola, M. W. Moskewicz, K. Ashraf, S. Han, W. J. Dally, and K. Keutzer. SqueezeNet: Alexnet-level accuracy with 50x fewer parameters and 1mb model size. *arXiv preprint arXiv:1602.07360*, 2016. 7
- [33] Y. Jia, E. Shelhamer, J. Donahue, S. Karayev, J. Long, R. Girshick, S. Guadarrama, and T. Darrell. Caffe: Convolutional architecture for fast feature embedding. In *Proceedings of the 22nd ACM international conference on Multimedia*, pages 675–678. ACM, 2014. 5
- [34] Z. Jia, A. Gallagher, A. Saxena, and T. Chen. 3d-based reasoning with blocks, support, and stability. In *Proceedings of the IEEE Conference on Computer Vision and Pattern Recognition*, pages 1–8, 2013. 1, 2
- [35] H. Jiang and J. Xiao. A linear approach to matching cuboids in rgbd images. In *Proceedings of the IEEE Conference on Computer Vision and Pattern Recognition*, pages 2171–2178, 2013. 3
- [36] A. Kar, S. Tulsiani, J. Carreira, and J. Malik. Category-specific object reconstruction from a single image. In *2015 IEEE Conference on Computer Vision and Pattern Recognition (CVPR)*, pages 1966–1974. IEEE, 2015. 3
- [37] A. Krizhevsky, I. Sutskever, and G. E. Hinton. Imagenet classification with deep convolutional neural networks. In *Advances in neural information processing systems*, pages 1097–1105, 2012. 2, 3
- [38] D. C. Lee, M. Hebert, and T. Kanade. Geometric reasoning for single image structure recovery. In *Computer Vision and Pattern Recognition, 2009. CVPR 2009. IEEE Conference on*, pages 2136–2143. IEEE, 2009. 3
- [39] J. J. Lim, A. Khosla, and A. Torralba. Fpm: Fine pose parts-based model with 3d cad models. In *European Conference on Computer Vision*, pages 478–493. Springer, 2014. 3
- [40] W. Liu, D. Anguelov, D. Erhan, C. Szegedy, and S. Reed. Ssd: Single shot multibox detector. In *ECCV*, 2016. 2, 3, 7
- [41] M. Rastegari, V. Ordonez, J. Redmon, and A. Farhadi. Xnor-net: Imagenet classification using binary convolutional neural networks. In *ECCV*, 2016. 7
- [42] J. Redmon, S. Divvala, R. Girshick, and A. Farhadi. You only look once: Unified, real-time object detection. In *CVPR*, 2016. 3
- [43] S. Ren, K. He, R. Girshick, and J. Sun. Faster r-cnn: Towards real-time object detection with region proposal networks. In *Advances in neural information processing systems*, pages 91–99, 2015. 2, 3, 5
- [44] L. G. Roberts. *Machine perception of three-dimensional soups*. PhD thesis, Massachusetts Institute of Technology, 1963. 3
- [45] S. Savarese and L. Fei-Fei. 3d generic object categorization, localization and pose estimation. In *2007 IEEE 11th International Conference on Computer Vision*, pages 1–8. IEEE, 2007. 3
- [46] T. Shao, A. Monszpart, Y. Zheng, B. Koo, W. Xu, K. Zhou, and N. J. Mitra. Imagining the unseen: Stability-based cuboid arrangements for scene understanding. *ACM Transactions on Graphics*, 33(6), 2014. 2
- [47] K. Simonyan and A. Zisserman. Very deep convolutional networks for large-scale image recognition. *arXiv preprint arXiv:1409.1556*, 2014. 5
- [48] S. Song and J. Xiao. Sliding shapes for 3d object detection in depth images. In *ECCV*, pages 634–651. Springer, 2014. 2
- [49] S. Song and J. Xiao. Deep sliding shapes for amodal 3d object detection in rgbd images. In *CVPR*, 2016. 2
- [50] H. Su, C. R. Qi, Y. Li, and L. J. Guibas. Render for cnn: Viewpoint estimation in images using cnns trained with rendered 3d model views. In *Proceedings of the IEEE International Conference on Computer Vision*, pages 2686–2694, 2015. 2
- [51] S. Tulsiani and J. Malik. Viewpoints and keypoints. In *IEEE Conference on Computer Vision and Pattern Recognition (CVPR)*, pages 1510–1519. IEEE, 2015. 2, 3
- [52] M. Wilczkowiak, P. Sturm, and E. Boyer. Using geometric constraints through parallelepipeds for calibration and 3d modeling. *IEEE transactions on pattern analysis and machine intelligence*, 27(2):194–207, 2005. 3
- [53] J. Wu, T. Xue, J. J. Lim, Y. Tian, J. B. Tenenbaum, A. Torralba, and W. T. Freeman. Single image 3d interpreter network. In *ECCV*, 2016. 2, 3
- [54] Y. Xiang, W. Choi, Y. Lin, and S. Savarese. Data-driven 3d voxel patterns for object category recognition. In *2015 IEEE Conference on Computer Vision and Pattern Recognition (CVPR)*, pages 1903–1911. IEEE, 2015. 3
- [55] J. Xiao, B. Russell, and A. Torralba. Localizing 3d cuboids in single-view images. In *Advances in neural information processing systems*, pages 746–754, 2012. 3, 5, 6, 7
- [56] Y. Yang and D. Ramanan. Articulated human detection with flexible mixtures of parts. *PAMI*, 35(12):2878–2890, 2013. 6
- [57] Y. Zheng, X. Chen, M.-M. Cheng, K. Zhou, S.-M. Hu, and N. J. Mitra. Interactive images: cuboid proxies for smart image manipulation. *ACM Trans. Graph.*, 31(4):99–1, 2012. 2